Published OnlineFirst February 26, 2014; DOI: 10.1158/1078-0432.CCR-13-1153

Imaging, Diagnosis, Prognosis

Clinical Cancer Research

Imaging the Norepinephrine Transporter in Neuroblastoma: A Comparison of [^{18}F]-MFBG and ^{123}I-MIBG

Hanwen Zhang[1], Ruimin Huang[1], Nai-Kong V. Cheung[2], Hongfen Guo[2], Pat B. Zanzonico[1,4], Howard T. Thaler[5], Jason S. Lewis[1,6], and Ronald G. Blasberg[1,3,6]

Abstract

Purpose: The norepinephrine transporter (NET) is a critical regulator of catecholamine uptake in normal physiology and is expressed in neuroendocrine tumors like neuroblastoma. Although the norepinephrine analog, meta-iodobenzylguanidine (MIBG), is an established substrate for NET, ^{123}I/^{131}I-MIBG has several clinical limitations for diagnostic imaging. In the current studies, we evaluated meta-[^{18}F]-fluorobenzylguanidine ([^{18}F]-MFBG) and compared it with ^{123}I-MIBG for imaging NET-expressing neuroblastomas.

Experimental Design: NET expression levels in neuroblastoma cell lines were determined by Western blot and ^{123}I-MIBG uptake assays. Five neuroblastoma cell lines and two xenografts (SK-N-BE(2)C and LAN1) expressing different levels of NET were used for comparative *in vitro* and *in vivo* uptake studies.

Results: The uptake of [^{18}F]-MFBG in cells was specific and proportional to the expression level of NET. Although [^{18}F]-MFBG had a 3-fold lower affinity for NET and an approximately 2-fold lower cell uptake *in vitro* compared with that of ^{123}I-MIBG, the *in vivo* imaging and tissue radioactivity concentration measurements demonstrated higher [^{18}F]-MFBG xenograft uptake and tumor-to-normal organ ratios at 1 and 4 hours after injection. A comparison of 4 hours [^{18}F]-MFBG PET (positron emission tomography) imaging with 24 hours ^{123}I-MIBG SPECT (single-photon emission computed tomography) imaging showed an approximately 3-fold higher tumor uptake of [^{18}F]-MFBG, but slightly lower tumor-to-background ratios in mice.

Conclusions: [^{18}F]-MFBG is a promising radiopharmaceutical for specifically imaging NET-expressing neuroblastomas, with fast pharmacokinetics and whole-body clearance. [^{18}F]-MFBG PET imaging shows higher sensitivity, better detection of small lesions with low NET expression, allows same day scintigraphy with a shorter image acquisition time, and has the potential for lower patient radiation exposure compared with ^{131}I/^{123}I-MIBG. *Clin Cancer Res; 20(8); 2182–91. ©2014 AACR.*

Introduction

Neuroblastoma is the most common extracranial solid cancer in childhood, with an annual incidence of about 650 cases per year in the United States (1–3). Approximately 50% of patients have metastatic disease at the time of diagnosis and are at high risk for relapse. Long-term survival among high-risk patients is generally less than 30% (4, 5). Neuroblastoma is derived from the neural crest progenitor cells and is classified as a neuroendocrine tumor; 90% of neuroblastomas overexpress the norepinephrine transporter (NET). The NET transmembrane protein is one of several monoamine transporters involved in the uptake of norepinephrine, epinephrine, and dopamine across the cell membrane (6). The expression and transporter function of NET provide the basis and rationale for the use of radiolabeled norepinephrine analogs for targeted imaging and treatment of neuroblastoma.

Meta-iodobenzylguanidine (MIBG) is a metabolically stable analog of norepinephrine (7), and ^{131}I-MIBG ($t_{1/2} = 8$ days; β^-, EC 97%; $E\gamma = 606$, 364 keV) has been widely used for the targeted imaging (single-photon emission computed tomography, SPECT/planar) and treatment of NET-expressing cancer for several decades (8, 9). ^{123}I-MIBG ($t_{1/2} = 13.3$ hours; EC 89%; $E\gamma = 159$ keV) was approved for diagnostic imaging in 2008, and is the current standard for clinical staging of neuroblastoma (10). However, both ^{123}I- and ^{131}I-MIBG have significant disadvantages as imaging tracers. These include (i) only semiquantitative measurements of

Authors' Affiliations: Departments of [1]Radiology, [2]Pediatrics, [3]Neurology, [4]Medical Physics, [5]Epidemiology and Biostatistics, and [6]Molecular Pharmacology and Chemistry Program, Memorial Sloan Kettering Cancer Center (MSKCC), New York, New York

Note: Supplementary data for this article are available at Clinical Cancer Research Online (http://clincancerres.aacrjournals.org/).

H. Zhang and R. Huang contributed equally to this article.

Corresponding Author: Ronald G. Blasberg, Memorial Sloan Kettering Cancer Center, 415 E68th Street, New York, NY 10065. Phone: 646-888-2211; Fax: 646-422-0408; E-mail: blasberg@neuro1.mskcc.org

doi: 10.1158/1078-0432.CCR-13-1153

Published OnlineFirst February 26, 2014; DOI: 10.1158/1078-0432.CCR-13-1153

Translational Relevance

The presence of metastatic disease is one of the strongest outcome prognostic factors for neuroblastoma, and sensitive imaging methods of tumor detection is the basis for accurate staging. Meta-iodobenzylguanidine (MIBG) scintigraphy is now a world-wide standard for defining the extent of disease at diagnosis, to monitor disease response during therapy, and to detect residual and recurrent disease during follow-up. However, both ^{123}I- and ^{131}I-MIBG scintigraphic/SPECT (single-photon emission computed tomography) imaging have limitations.

We hypothesized that meta-[^{18}F]fluorobenzylguanidine ([^{18}F]-MFBG), a more hydrophilic benzylguanidine analog than MIBG, should have lower binding to plasma proteins and would be cleared more rapidly from nontarget tissues and from the body, and that this would result in superior tumor-to-background ratios at earlier times after administration. Shorter image acquisition times will facilitate the logistics of imaging in the pediatric population and improved tumor detection would likely result from the use of (positron emission tomography) PET compared with SPECT. Our studies confirm these hypotheses and demonstrate that PET imaging with [^{18}F]-MFBG is a promising technique to quantitatively measure norepinephrine transporter expression in neuroblastoma.

$^{123/131}$I-MIBG tumor accumulation by routine single-photon imaging; (ii) the inability to detect small metastatic lesions; (iii) the potential for false-positive identification of metastasis due to high background and limited spatial resolution (11–13); (iv) inconvenience of multiple hospital visits (injection of the radiopharmaceutical and next-day imaging). Consequently, a benzylguanidine analog labeled with positron emitter would be more useful for initial staging of neuroblastoma, and for the evaluation of treatment response (10) and detection of recurrent disease (2). A positron emission tomography (PET) radiopharmaceutical would likely provide greater sensitivity and superior resolution for lesion detection, a shorter image acquisition time facilitating pediatric studies, and potentially lower radiation exposure. Among the potential radioisotopes (^{124}I, ^{76}Br, ^{18}F, and ^{11}C) that are suitable for labeling benzylguanidine analogs, ^{18}F-fluoride is the most promising radioisotope due to its wide availability, low cost, and optimal physical half-life for same-day imaging.

In this study, we (i) screen a panel of neuroblastoma cell lines for NET expression and correlate the results with ^{123}I-MIBG uptake studies; (ii) evaluate meta-[^{18}F]fluorobenzylguanidine ([^{18}F]-MFBG) for imaging in neuroblastoma cells and xenografts with different endogenous levels of NET expression; and (iii) perform a direct comparison of [^{18}F]-MFBG with ^{123}I-MIBG (clinical formulation) for imaging NET expression. Our studies demonstrate that PET imaging with [^{18}F]-MFBG provides better images and a more quantitative measurement of NET expression in neuroblastoma animal models than ^{123}I-MIBG single-photon SPECT imaging.

Materials and Method

General

All chemicals were obtained from commercial sources and were used without further purification. [^{18}F]-MFBG (~19 GBq/μmol) was synthesized at Memorial Sloan Kettering Cancer Center (MSKCC). ^{123}I-MIBG (~0.31 GBq/μmol) was obtained from Nuclear Diagnostics Products. Neuroblastoma cell lines, including SK-N-BE(2)C, SK-N-BE(2)N, SK-N-BE(1)N, and SK-N-SH were derived at MSKCC, and LAN1 was kindly provided by Dr. Robert Seeger (Children's Hospital of Los Angeles, CA); they were all cultured using RPMI-1640 medium with 10% FBS (HyClone). Radioactivity was measured using an appropriately calibrated WIZARD 3″ 1480 γ-counter (PerkinElmer) or a dose calibrator (CAPINTEC CRC-30BC).

Screening of NET expression in neuroblastoma cell lines

Immunoblots. Total protein was isolated using the radioimmunoprecipitation assay buffer (Millipore) following the manufacturer's instruction. Twenty-five micrograms of the total protein was run on a precast 4% to 12% SDS-PAGE gel (Invitrogen), electrophoretically transferred to a polyvinylidene difluoride membrane and blotted with an anti-NET antibody (1:2,000; NET17-1; MAb Technologies) and an anti–β-actin antibody (1:5,000; ab6276; Abcam). The blots were visualized using the Western Lighting Plus-ECL (PerkinElmer). The density of Western blot band was quantified using the Image J software (NIH).

Competitive inhibition of MFBG and MIBG binding to the NET. Competitive affinity studies were performed in SK-N-BE(2)C cells using ^{123}I-MIBG and various concentrations of MIBG and MFBG. Triplicate samples containing approximately 0.5×10^6 cells, approximately 3.7 kBq ^{123}I-MIBG, and 0.005 to 50 nmol MFBG (or MIBG) in 0.5-mL cell culture medium were incubated at 37°C for 2 hours. The cells were collected with glass microfiber filters, washed with 3×2 mL of ice-cold TBS (pH 7.4), and radioassayed with a γ-counter. ^{123}I-MIBG uptake in SK-N-BE(2)C cells was plotted versus the MFBG (or MIBG) concentration, and IC_{50} values were estimated using a least-squares fitting routine (GraphPad Prism 5).

Uptake of ^{123}I-MIBG and ^{18}F-MFBG. Triplicate samples contained approximately 11.1 kBq of ^{18}F-MFBG or 3.7 kBq of ^{123}I-MIBG and 1.0×10^6 cells in a total volume of 1.0-mL cell culture medium. The samples were gently shaken at 37°C for 2 hours. Two hundred micromole per liter of MIBG or 50 μmol/L of desipramine (final concentration) were used in blocking experiments to determine the specificity of accumulation. After incubation, the cells were collected and analyzed using the method described above for the competitive inhibition studies. For kinetic uptake studies, the samples were gently shaken at 37°C for 5, 20, 50, and 120

Published OnlineFirst February 26, 2014; DOI: 10.1158/1078-0432.CCR-13-1153

minutes. The uptakes of [^{18}F]-MFBG and ^{123}I-MIBG were plotted versus time of incubation and analyzed using a one-component kinetic model.

In vivo imaging

All animal experiments were approved by the Institutional Animal Care and Utilization Committee of MSKCC. Neuroblastoma cells were suspended in 200 μL of cell culture medium/Matrigel (BD Bioscience; v/v = 1/1). SK-N-BE(2)C (2×10^6) or LAN1 (10×10^6) cells were injected subcutaneously in the left shoulder of female athymic Ncr-nu/nu mice (7- to 9-week-old; Taconic). Twenty to 30 days after the inoculation, tumors were approximately 200 mm^3 in size, and imaging and tissue sampling studies were performed.

PET and PET/CT imaging with [^{18}F]-MFBG. For PET imaging studies ($n = 12$ animals for SK-N-BE(2)C and $n = 10$ animals for LAN1 xenografts; Fig. 5A), [^{18}F]-MFBG (3.7 to 11.1 MBq in 100 to 200 μL saline) was injected through the tail vein. PET imaging was performed at 1 and 4 hours p.i. on a R4 microPET scanner (Concorde Microsystems; ref. 14), with the tumors centered in the field of view, and the animal under 2% isoflurane anesthesia. Ten-minute acquisitions were collected with an energy window of 350 to 750 keV and a coincidence timing window of 6 ns. A three-dimensional (3D) volume-of-interest (VOI) analysis of the acquired images was performed using ASIPro software (Siemens), and the observed mean radioactivity concentration (%ID/cc) derived.

For PET/CT imaging studies ($n = 5$ animals for both SK-N-BE(2)C and LAN1 xenografts; Fig. 4), the animal was immobilized in a home-made restraint device for the co-registration of PET and CT (X-ray computed tomography) imaging data. After 15 minutes of data acquisition on PET (Focus 120 microPET scanner), the animal was moved to a microCAT II (ImTek Inc.) scanner under 2% isoflurane anesthesia. CT acquisition was performed for 10 minutes at 60 kVp and 0.8 mA with 2-mm aluminum filtration. PET images were reconstructed by both maximum *a priori* and 3D filtered back-projection, and the reconstruction using a ramp filter with a cutoff frequency was equal to the Nyquist frequency into a $128 \times 128 \times 95$ matrix. The reconstructed data of PET and CT images were rendered in 3D using Amira 5.0 (Visage Imaging GmbH) or Inveon Research Workstation (Siemens).

SPECT/CT imaging with ^{123}I-MIBG. The same group of animals imaged with PET/CT was also imaged by SPECT/CT the following day. Animals were administrated 18.5 to 44.4 MBq of ^{123}I-MIBG through the tail vein, and imaging was performed at 1, 4, and 24 hours p.i. on a NanoSPECT/CT Plus scanner (BIOSCAN). CT data were acquired for 8 to 10 minutes at a 45-kVp voltage and 500-ms exposure before each SPECT scan. The SPECT image parameters were 1.0 mm/pixel, 256×256 frame size, and 70 to 90 s per projection with a total of 24 projections. The acquisition time was approximately 60 minutes at 1 hour, 90 minutes at 4 hours, and 170 minutes at 24 hours p.i. During imaging, the animal was anesthetized with 1.5% isoflurane in 2.0 L/min O_2 and the body temperature was maintained with warm air (37°C). InVivoScope 1.37 software (Bioscan) was used for reconstruction. A color threshold was optimized to visualize tumor clearly on the SPECT/CT fusion image.

Immunohistochemistry staining for NET expression. The neuroblastoma xenografts were collected from the imaging studies and fixed by formalin. Paraffin-embedded tissue sections (5 μm) were immunostained using the Discovery XT biomarker platform (Ventana). The primary antibody, anti-SLC6A2/NET polyclonal antibody (MBL; BMP029), was diluted at 1:100. Biotin-labeled anti-rabbit antibody (1:300; BA-1000; Vector Laboratories;) was used as the secondary antibody.

Radiation exposure (absorbed dose estimates)

Data from the murine biodistribution studies of [^{18}F]-MFBG and ^{123}I-MIBG (Supplementary Tables S1 and S2) and from human ^{123}I-MIBG SPECT imaging studies in patients were each fitted to an exponential function using least-squares regression (Excel; Microsoft Corp.). The fitted time-activity concentration functions were integrated (incorporating the effect of the physical decay of ^{18}F, ^{123}I, and ^{124}I) and converted from concentrations to total-organ values using the 33-kg 10-year-old child organ masses to yield the respective organ residence times (h). The rest-of-body residence time was calculated as the difference between the total-body residence time and the sum of the normal-organ residence times. For walled organs (heart, large intestine, small intestine, stomach, and urinary bladder), the residence time was assigned entirely to the organ contents, with the large intestine residence time divided evenly between the upper and lower large intestines. The bone residence time was likewise evenly divided between cortical and trabecular bone. The red marrow cumulated activity was estimated from the blood residence time, assuming instantaneous equilibration of MFBG (or MIBG) between plasma and marrow extracellular space, a plasmacrit of 0.6, and a marrow fractional extracellular space of 0.4. Finally, the mean normal-organ radiation doses (cGy/MBq administered) and the effective dose (cSv/MBq administered) for [^{18}F]-MFBG, ^{123}I-MIBG, and [^{124}I]-MIBG were calculated for a 33-kg standard anatomic model (10-year-old child equivalent) and the medical internal radiation dose "(MIRD) formalism," as implemented in the OLINDA EXM program.

Statistical analysis

The mouse xenograph data presented comprise results of several factorial experiments to compare the uptake of two radioactive probes (^{123}I-MIBG vs. [^{18}F]-MFBG), in two tumor types (SK-N-BE(2)C vs. LAN1), time elapsed from probe administration (5 minutes, 20 minutes, 1 hour, 4 hours, and 24 hours) and data acquisition modality (biodistribution vs. PET). Biodistribution (Bio-D) measurements of tumors were made only once per mouse (sacrifice is required to obtain specimens), whereas PET allows repeated measurements at successive time points in the same mouse. The factorial designs comprised independent experiments with the exception that [^{18}F]-MFBG biodistribution measurements for SK-N-BE(2)C at 1 and 4 hours

Published OnlineFirst February 26, 2014; DOI: 10.1158/1078-0432.CCR-13-1153

Table 1. Estimated surface integral exposure (absorbed radiation dose) following the administration of [^{18}F]-MFBG, ^{123}I-MIBG, and [^{124}I]-MIBG to a 33 kg of standard person (child) using the MIRD formalism[a]

	Radiation dose ($\times 10^{-3}$ cGy/MBq)			
Tissue	[^{18}F]-MFBG[b]	^{123}I-MIBG[b]	^{123}I-MIBG[c]	[^{124}I]-MIBG[c]
Adrenals	1.19	0.86	1.14 ± 0.27	17.2 ± 3.0
Brain	0.22	0.08	0.60 ± 0.14	8.38 ± 1.89
Breasts	0.78	0.22	0.62 ± 0.14	10.3 ± 1.9
Gallbladder wall	1.41	0.70	1.46 ± 0.35	19.7 ± 3.8
Lower large intestine wall	2.76	0.97	0.73 ± 0.16	10.5 ± 2.4
Small intestine	2.30	1.89	0.87 ± 0.19	13.0 ± 2.4
Stomach wall	2.30	0.73	0.95 ± 0.22	13.0 ± 2.4
Upper large intestine wall	1.86	0.86	0.92 ± 0.22	13.5 ± 2.4
Heart wall	3.00	1.27	3.14 ± 0.89	48.4 ± 14.6
Kidneys	1.24	0.68	0.92 ± 0.22	14.1 ± 2.4
Liver	2.70	1.32	4.16 ± 0.13	73.0 ± 18.4
Lungs	1.00	0.40	2.41 ± 0.51	36.5 ± 7.8
Muscle	0.86	0.32	0.68 ± 0.14	10.3 ± 7.8
Ovaries	2.27	0.95	7.84 ± 0.16	11.6 ± 2.4
Pancreas	1.41	0.78	1.16 ± 0.27	17.3 ± 3.0
Red marrow	1.35	0.51	0.62 ± 0.14	9.73 ± 1.89
Bone	1.78	1.16	2.03 ± 0.43	13.5 ± 2.7
Skin	0.78	0.22	0.43 ± 0.11	7.57 ± 1.62
Spleen	1.16	0.62	0.81 ± 0.16	12.2 ± 2.2
Testes	2.11	0.65	0.54 ± 0.11	8.65 ± 1.89
Thymus	1.00	0.30	0.81 ± 0.16	11.9 ± 2.4
Thyroid	0.91	0.27	0.70 ± 0.14	10.3 ± 2.2
Urinary bladder wall	46.5	11.9	0.70 ± 0.16	9.73 ± 1.89
Uterus	4.05	1.62	7.84 ± 0.16	11.6 ± 2.4
Total body	1.27	0.43	0.84 ± 0.19	12.7 ± 2.2
Effective dose ($\times 10^{-3}$ cSv/MBq)	3.97	1.24	1.08 ± 0.24	16.8 ± 3.0

[a]A typical dose of ^{123}I-MIBG is 5.2 MBq/kg. The predicted dose for [^{18}F]-MFBG is <3.7 MBq/kg, and for [^{124}I]-MIBG the dose is 3.7 MBq/kg.
[b]Estimated from radioactivity–time biodistribution studies of [^{18}F]-MFBG and ^{123}I-MIBG in mice (Supplementary Tables S1 and S2).
[c]Estimated from ^{123}I-MIBG SPECT/CT imaging studies of 19 patients at 0.8, 24.8, and 44.8 hours p.i..

were used both in the probe × tumor type × time analysis and in the biodistribution versus PET comparison. Both types of measurement had skewed statistical distributions within and across experimental conditions. Thus, statistical analyses were performed using log-transformed measurements as the outcome, or dependent variable. This reduced the effects of potential outliers and allowed data to more closely conform to implicit assumptions of the statistical methods. We could partition the time curve for each probe into mean, linear, quadratic, and cubic components and test whether there were differences between the two probes.

Data on estimated surface integral exposure (absorbed radiation dose) in Table 1 for humans and Supplementary Tables S1 and S2 for mouse xenografts are presented for descriptive purposes only, without statistical significance comparisons. Thus, they are reported as simple mean ± SD, calculated using Microsoft Excel. In mouse experiments, statistical significance for comparisons of prior interest between two specific combinations of experimental conditions [xenograph, data acquisition method, probe, and time post injection (p.i.)] is reported based on Student *t* tests of log-transformed measurements (a two-sample test when comparing or observations in two sets of animal or a paired test when comparing two measurements in the same animals). When assessing statistical significance for trends involving several combinations of experimental conditions, ANOVA F tests were used. For example, when comparing the two probes in SK-N-BE(2)C xenografts from 5 minutes to 4 hours, the time effect was parsed into linear, quadratic, and cubic effects using orthogonal polynomials. Values of $P < 0.05$ were considered statistically significant.

Results

Screening for NET expression in neuroblastoma cell lines

The expression of NET in five human neuroblastoma cell lines was assessed using ^{123}I-MIBG uptake and Western

Published OnlineFirst February 26, 2014; DOI: 10.1158/1078-0432.CCR-13-1153

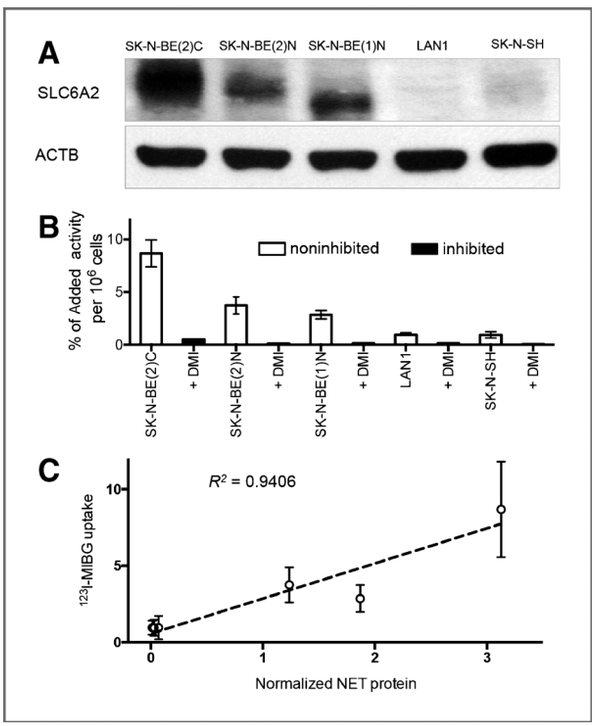

Figure 1. The expression of NET protein in neuroblastoma cell lines. A, expression of NET protein was detected by Western blot analysis using the α-SLC6A2/NET antibody. β-Actin was used as a loading control. A representative of four separate blots is shown. B, ^{123}I-MIBG *in vitro* uptake studies (open bar) and desipramine (DMI; 50 μmol/L) blocking experiments (closed bar). The results (mean ± SD) were from 2 to 6 independent studies with triplicates in each experiment. ($n = 6$ for SK-N-BE(2)C; $n = 2$ for SK-N-BE(2)N; $n = 5$ for SK-N-BE(1)N; $n = 6$ for LAN1; $n = 3$ for SK-N-SH; and $n = 2$ for blocking studies). C, correlation between ^{123}I-MIBG uptake and normalized NET protein (optical density ratio of the SLC6A2 and ACTB bands).

blotting assays (Fig. 1). Both assays showed that the endogenous expression of NET in SK-N-BE(2)C cells was high, moderate in SK-N-BE(2)N and SK-N-BE(1)N cells, and low in LAN1 and SK-N-SH cells (Fig. 1A and B). The ^{123}I-MIBG uptake results were consistent with endogenous NET expression levels, as determined by Western blotting analysis (Fig. 1C). Both MFBG and MIBG (Fig. 2) showed high competitive affinity (IC_{50}: MFBG: 3.29 ± 0.62 μmol/L; MIBG: 1.23 ± 0.17 μmol/L) to NET endogenously expressed in SK-N-BE(2)C cells. A representative competitive uptake curve is shown in Fig. 2.

[^{18}F]-MFBG and ^{123}I-MIBG uptake in different NET-expressing neuroblastoma cell lines

In vitro [^{18}F]-MFBG uptake studies were performed in four neuroblastoma cell lines, and showed corresponding high uptake in SK-N-BE(2)C, moderate uptake in SK-N-BE(2)N and SK-N-BE(1)N, and low uptake in LAN1 cells (Fig. 3A, open bars). These results can be directly compared with those obtained with ^{123}I-MIBG (Fig. 3B) and the NET expression levels (Fig. 1C). The uptake of ^{123}I-MIBG was always higher than that of [^{18}F]-MFBG in all tested cell lines (Figs. 1B and 3A). The time-dependent uptake of [^{18}F]-MFBG and ^{123}I-MIBG was measured in SK-N-BE(2)C cells. The data were analyzed with a one-compartment kinetic model (Fig. 3C). The results showed that the 3-fold higher uptake of ^{123}I-MIBG (Vd) compared with that of [^{18}F]-MFBG was primarily due to its more rapid influx (k1; Fig. 3D). This observation was consistent with the difference in IC_{50} values for the two tracers (Fig. 2). Blocking experiments with an excessive amount of "cold" MIBG or a NET inhibitor (desipramine) demonstrated that both ligands have a similarly high specificity toward NET (Figs 1B and 3A).

In vivo imaging and biodistribution

[^{18}F]-MFBG PET/CT and ^{123}I-MIBG SPECT/CT images were obtained in the same animals bearing NET-expressing neuroblastoma xenografts at 1 and 4 hours p.i., and at 24 hours p.i. for ^{123}I-MIBG only (Fig. 4). [^{18}F]-MFBG clearly delineated SK-N-BE(2)C xenografts (high NET expression) from the adjacent background radioactivity in the images at both 1 and 4 hours time points (Fig. 4A). [^{18}F]-MFBG radioactivity was also visible in normal organs, including brown fat, liver, and intestine, at 1 hour p.i.; however, at 4 hours p.i., most organ radioactivity was low, resulting in high tumor-to-background ratios (Supplementary Table S1). Coregistered PET/CT imaging showed high specific accumulation of [^{18}F]-MFBG in the SK-N-BE(2)C xenografts (high NET expression) and in salivary glands and the bladder (Fig. 4A and C). LAN1 xenografts (low NET expression) were also visualized with [^{18}F]-MFBG imaging (Fig. 4B

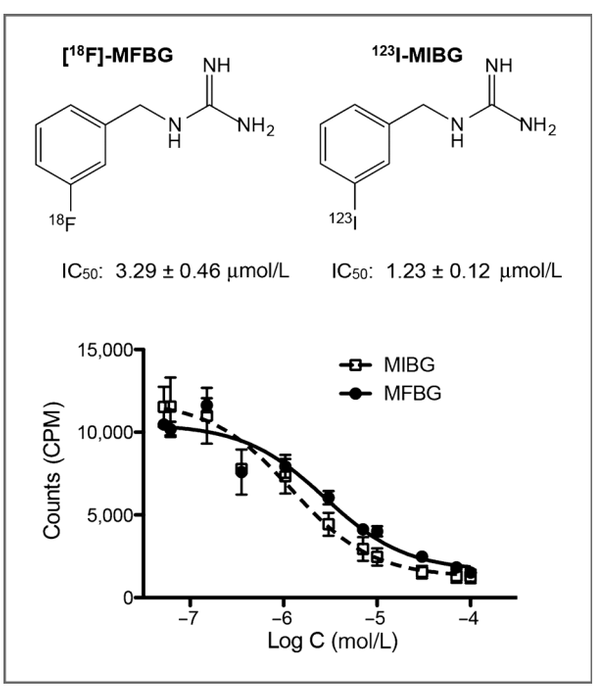

Figure 2. Structures of [^{18}F]-MFBG and ^{123}I-MIBG and their competitive inhibition of ^{123}I-MIBG binding to the NET. The IC_{50} values (mean ± SD) were determined in SK-N-BE(2)C cells; four (MFBG) and two (MIBG) independent studies were performed, with triplicates in each experiment.

Published OnlineFirst February 26, 2014; DOI: 10.1158/1078-0432.CCR-13-1153

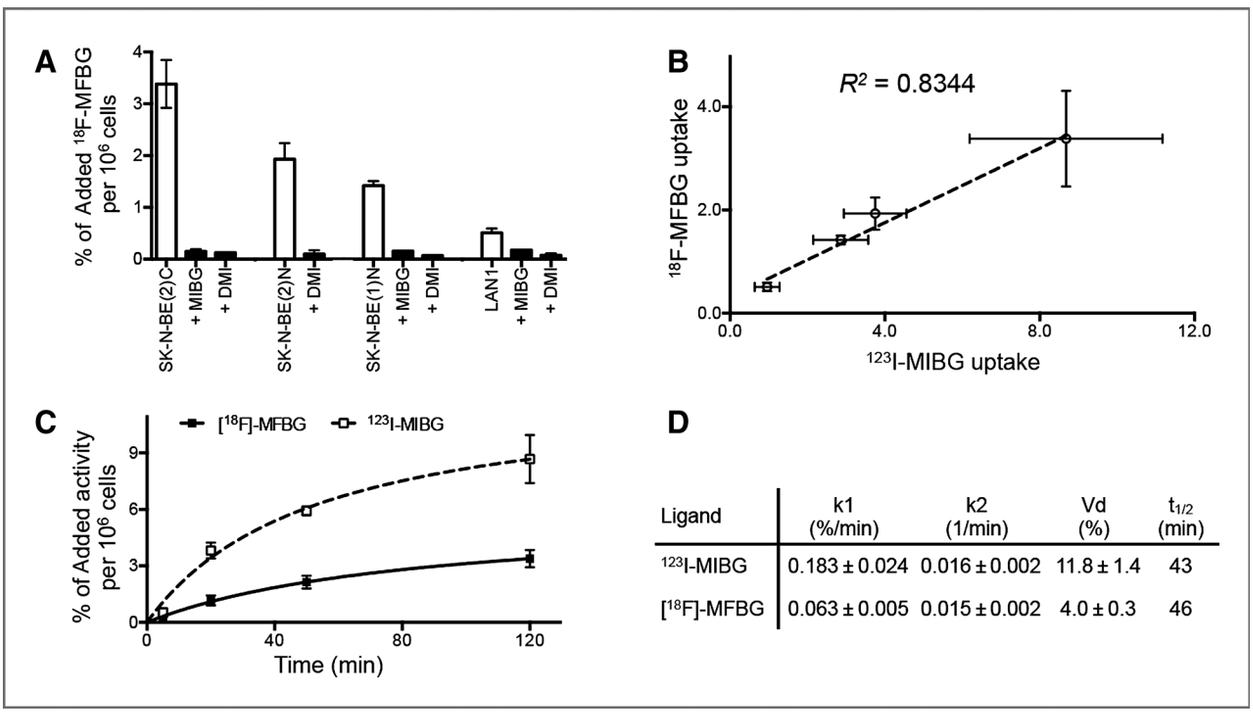

Figure 3. An *in vitro* uptake of [^{18}F]-MFBG and ^{123}I-MIBG. A, [^{18}F]-MFBG uptake in neuroblastoma cell lines (open bars) could be blocked by either MIBG (200 μmol/L) or desipramine (50 μmol/L; closed bars). Values (mean ± SD) from 2 to 5 independent studies with triplicates in each experiment: $n = 5$ for SK-N-BE(2)C; $n = 2$ for SK-N-BE(2)N; $n = 2$ for SK-N-BE(1)N; $n = 3$ for LAN1; and $n = 2$ for blocking experiments. B, correlation between [^{18}F]-MFBG and ^{123}I-MIBG uptake (data from Figs. 3A and 1B, respectively; slope, 0.36 ± 0.05; Y-intercept, 0.32 ± 0.30). C and D, kinetic analysis of [^{18}F]-MFBG and ^{123}I-MIBG uptake in SK-N-BE(2)C cells (two independent studies, with triplicates in each experiment). A one-compartment kinetic analysis of the radioactivity–time data was performed.

and D), although the images showed less contrast due to the lower tumor uptake. 3D VOI values (%ID/mL) of [^{18}F]-MFBG obtained from the PET images confirmed significantly higher uptake of [^{18}F]-MFBG in SK-N-BE(2)C xenografts compared with that in LAN1 xenografts at the 1 and 4 hours p.i. time points ($P < 0.0001$; Fig. 5A). Paired PET measurements were slightly higher at 4 hours than at 1 hour p.i. for SK-N-BE(2)C ($P = 0.017$), and slightly lower for LAN1 xenografts ($P = 0.009$). Tumor sampling and radioactivity (well counter) measurements (%ID/g; Supplementary Table S1) yielded similar results to those obtained with VOI PET (%ID/mL; Fig. 5A); there were no significant differences between paired biodistribution and VOI PET measurements at the 4 hours p.i. time point. ($P > 0.7$ for both xenographs). ANOVA showed that the biodistribution measurements for both [^{18}F]-MFBG and ^{123}I-MIBG in SK-N-BE(2)C xenografts increased at a similar ($P = 0.666$) rate from 5 minutes to 4 hours on a log-log scale (1.33-fold increase for ^{123}I-MIBG and 1.24-fold increase for [^{18}F]-MFBG, per 4-fold increase in hours elapsed, $P = 0.0027$ overall), and that [^{18}F]-MFBG yielded 27.3% proportionally higher values than ^{123}I-MIBG across the 4-hour time period ($P = 0.025$).

^{123}I-MIBG NanoSPECT/CT imaging of SK-N-BE(2)C xenografts at 1 and 4 hours p.i. showed lower tumor-to-background contrast, with greater retention in the liver, gall bladder, and intestine compared with [^{18}F]-MFBG at 1 and 4 hours (Fig. 4A). This was consistent with the higher hydrophobicity and slower body clearance of ^{123}I-MIBG compared with [^{18}F]-MFBG. However, a significant improvement in ^{123}I-MIBG SPECT/CT image quality of SK-N-BE(2)C xenografts was observed at 24 hours p.i. (Fig. 4C). In contrast, LAN1 xenografts could not be imaged consistently at either 4 or 24 hours p.i. (Fig. 4B and D), due to a low tumor uptake (Supplementary Table S2) that was indistinguishable from surrounding background.

The results of the biodistribution (tissue sampling and well-counting) studies (Supplementary Tables S1 and S2) confirmed the PET and SPECT imaging results (Figs 4 and 5A), and the difference in NET expression in SK-N-BE(2)C and LAN1 xenografts was also confirmed by immunohistochemical staining (Fig. 5B).

Radiation exposure: absorbed dose estimates

The normal-organ radiation exposure (cGy/MBq) and the effective dose (cSv/MBq) of [^{18}F]-MFBG, ^{123}I-MIBG, and [^{124}I]-MIBG for a 33-kg child were calculated and are presented in Table 1. On the basis of the mouse biodistribution data (Supplementary Tables S1 and S2), the normal-organ absorbed doses are quite low (<0.003 cGy/MBq), except for the urinary bladder wall (0.047 cGy/MBq). In comparison with adult human data (based on unpublished ^{123}I-MIBG SPECT/CT imaging studies of 19 patients), both [^{18}F]-MFBG and ^{123}I-MIBG showed a similar absorbed dose

Published OnlineFirst February 26, 2014; DOI: 10.1158/1078-0432.CCR-13-1153

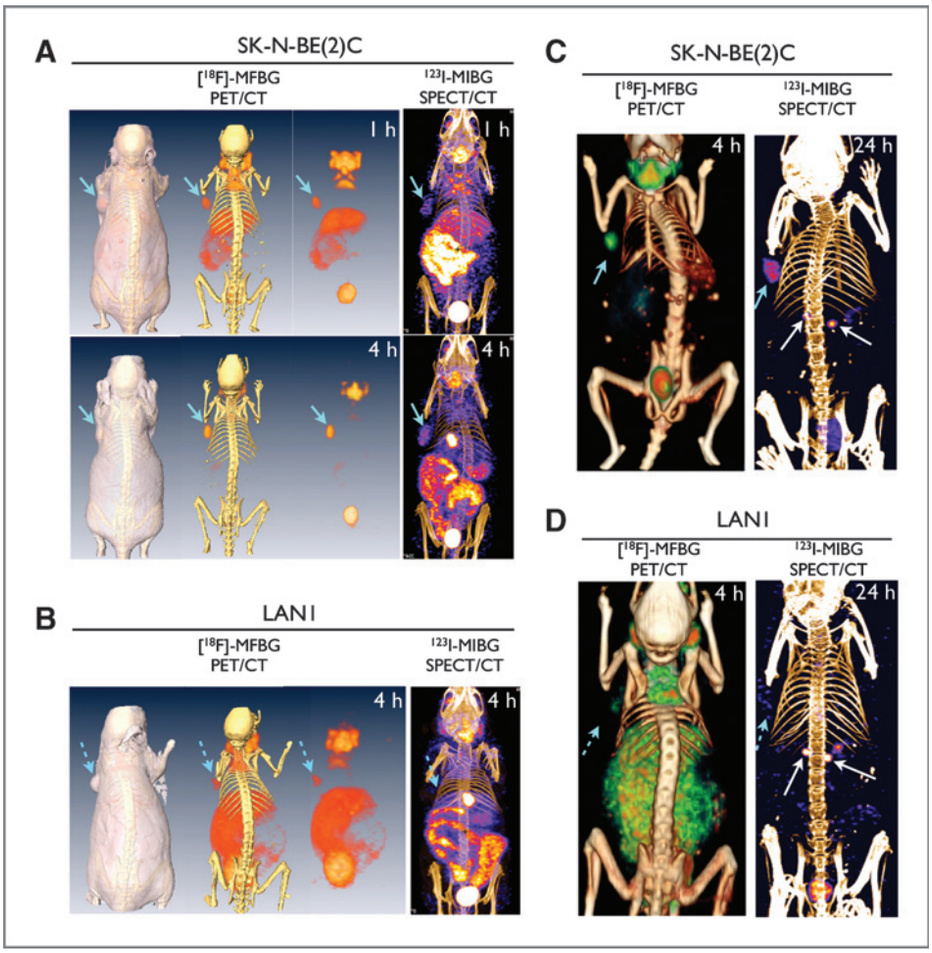

Figure 4. Neuroblastoma xenografts imaged in the same animal with [^{18}F]-MFBG (PET/CT) and ^{123}I-MIBG (SPECT/CT). A, SK-N-BE(2)C tumor-bearing mice ($n = 7$) were imaged at 1 and 4 hours p.i. with [^{18}F]-MFBG on day 1 and with ^{123}I-MIBG on day 2. B, LAN1 tumor-bearing mice ($n = 5$) were imaged at 1 and 4 hours p.i. with [^{18}F]-MFBG on day 1 and with ^{123}I-MIBG on day 2. C and D, two additional sets of SK-N-BE(2)C ($n = 5$) and LAN1 ($n = 5$) tumor-bearing mice, respectively, were imaged at 4 hours p.i. with [^{18}F]-MFBG on day 1, and then with ^{123}I-MIBG at 24 hours p.i. on day 3. A color threshold was optimized to visualize the tumor clearly on the fusion image. An accurate color intensity scale bar (%ID/cc) is precluded in these MIP (maximum intensity projection) images (VOI measurements are provided in Fig 5A). [^{18}F]-MFBG PET visualized SK-N-BE(2)C xenografts (solid arrow) with high tumor-to-background contrast, especially at 4 hours p.i. ^{123}I-MIBG SPECT imaging shows poor tumor-to-background contrast at both 1 and 4 hours, but a significantly improved image was observed at 24 hours (the two adrenal glands were clearly visualized). LAN1 xenografts (dash arrow) could be detected by [^{18}F]-MFBG PET at 4 hours p.i., but not by ^{123}I-MIBG SPECT at 24 hours p.i.

(cGy/MBq) in most organs, and these were 5- to 10-fold lower than those for ^{124}I-MIBG. The estimated absorbed doses based on the ^{123}I-MIBG patient data were slightly higher than those based on the mouse biodistribution data, except for the urinary bladder. The effective radiation dose for [^{18}F]-MFBG (0.00397 cSv/MBq) was approximately 3-fold higher than that for ^{123}I-MIBG, and approximately 4-fold lower than ^{124}I-MIBG (0.0168 ± 0.00297 cSv/MBq).

Discussion

The presence of metastatic disease is one of the most reliable prognosticators of neuroblastoma outcome (15), and sensitive and specific methods to detect metastases are thus critical for accurate staging (10). Furthermore, the ability to detect early relapse may be critical if patients are to be successfully salvaged after progression (2). MIBG scintigraphy has played an important role in the diagnosis and therapy of neuroblastoma (16). It is now a standard of care worldwide for defining the extent of disease at diagnosis, to monitor disease response during therapy, and to detect residual and recurrent disease during follow-up (8, 17, 18). MIBG is sensitive and specific for neuroblastoma, concentrating in >90% of tumors. Although ^{131}I-MIBG was initially used, ^{123}I-MIBG has yielded better quality images at a lower patient radiation dose and was approved for clinical use in children by the U.S. Food and Drug Administration in 2008. However, both ^{123}I- and ^{131}I-MIBG scintigraphic/SPECT imaging have limitations (19).

To address some of the limitations associated with $^{123/131}$I-MIBG imaging of NET overexpression in neural crest and neuroendocrine tumors and to evaluate a probe for PET imaging, several [^{18}F]-labeled benzylguanidine analogs have been developed; these include [^{18}F]-FIBG (20), [^{18}F]-FPBG (21), and LMI1195 (22). Most of these ligands were designed to have a LogP value that was similar to that of MIBG, with the objective of achieving an *in vitro* uptake and an *in vivo* distribution similar to that of MIBG. The results in normal rodents showed that these MIBG analogs were partially excreted through the liver and digestive track, similar to MIBG. However, none of these [^{18}F]-labeled MIBG analogs were validated by imaging NET expression in xenografts, especially with respect to characterizing their pharmacokinetics *in vivo* or determining the optimal time for imaging to achieve maximum target-to-background ratios. Because an *in vitro* uptake was used previously as the sole criteria for choosing the "ideal" imaging ligand, the more hydrophilic benzylguanidine

Published OnlineFirst February 26, 2014; DOI: 10.1158/1078-0432.CCR-13-1153

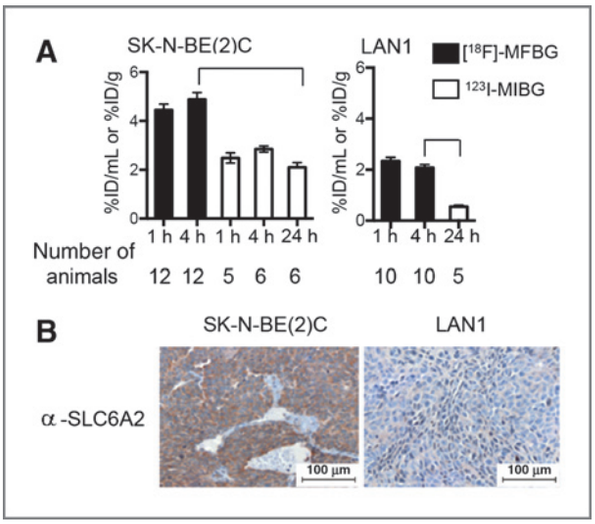

Figure 5. Quantitative measurements of neuroblastoma xenograft radioactivity. A, voxel-based 3D VOI values (%ID/mL) of [^{18}F]-MFBG were obtained from the PET images of SK-N-BE(2)C and LAN1 xenografts. ^{123}I-MIBG radioactivity measurements (%ID/g) were obtained from tissue dissection and γ well-counting. B, *ex vivo* immunohistochemistry staining of SK-N-BE(2)C and LAN1 xenografts. The VOI measurements of xenograft [^{18}F]-MFBG radioactivity are very similar to the values obtained by tissue dissection with γ well-counting in the biodistribution studies that were performed in different sets of animals (see Supplementary Table S1). The difference between 4-hour [^{18}F]-MFBG and 24-hour ^{123}I-MIBG uptake in SK-N-BE(2)C xenografts was highly significant ($P < 0.001$); similarly for LAN1 xenografts ($P < 0.001$). The difference in the expression of NET in SK-N-BE(2)C and LAN1 xenografts was confirmed by immunohistochemistry staining.

analogs were initially abandoned because they exhibited an inferior *in vitro* uptake in neuroblastoma and other test cell lines. We hypothesized that the more hydrophilic [^{18}F]-labeled benzylguanidine analogs should have a lower binding to plasma proteins and would be cleared more rapidly from nontarget tissues and from the body compared with the more hydrophobic MIBG. Thus, a high tumor-to-background ratio presumably could be achieved at an "early time."

The *in vitro* and *in vivo* results reported here support the foregoing hypotheses. Even though the more hydrophilic [^{18}F]-MFBG showed a 2- to 3-fold lower tumor cell uptake *in vitro* compared with that of ^{123}I-MIBG, the uptake of both [^{18}F]-MFBG and ^{123}I-MIBG in neuroblastoma cells was specific and corresponded to the expression level of NET. The observed lower uptake of [^{18}F]-MFBG compared with that of ^{123}I-MIBG in the four neuroblastoma cell lines reflects a lower affinity of [^{18}F]-MFBG for NET compared with ^{123}I-MIBG. Nevertheless, the correlation between tracer uptake and amount of NET protein demonstrates that [^{18}F]-MFBG is able to quantitatively measure NET expression levels.

In vivo studies showed that [^{18}F]-MFBG was able to clearly visualize neuroblastoma xenografts at 1 hour p.i., with the uptake in the tumor correlated with the expression level of NET. Tumor values tended to plateau after 1 hour, and a further increase in tumor/background contrast was achieved largely by whole-body radioactivity clearance. In contrast with the *in vitro* data, [^{18}F]-MFBG accumulation in SK-N-BE(2)C xenografts was approximately 2-fold greater than that of ^{123}I-MIBG, and background radioactivity levels in non-NET expressing organs were considerably less (~50%) at 4 hours p.i.. The lower background values reflected the more rapid body clearance of [^{18}F]-MFBG compared with that of ^{123}I-MIBG. The combined effect of greater uptake and more rapid body clearance resulted into an approximately 4-fold higher target-to-background ratio in SK-N-BE(2)C xenografts for [^{18}F]-MFBG than for ^{123}I-MIBG. The comparatively slow clearance of ^{123}I-MIBG relative to [^{18}F]-MFBG we observed in the mouse is likely to be greater in patients, because the serum free- (nonprotein bound) fraction of MIBG in human serum (12% ± 1%) is 2.4-fold less than that in murine serum (29% ± 2%), and significantly less than that of MFBG in both species (67% ± 1% and 70% ± 3%, for human and murine serum, respectively; ref. 23).

^{123}I-MIBG tumor-to-background specificity was substantially improved by imaging SK-N-BE(2)C xenografts at 1 day p.i., with intervening nontarget background/organ clearance of radioactivity. Because ^{123}I-MIBG SPECT imaging of patients with neuroblastoma is usually performed 1 day p.i., a comparison of 4-hour [^{18}F]-MFBG with 24-hour ^{123}I-MIBG is more clinically relevant. Our results showed a comparable image contrast for high NET-expressing SK-N-BE(2)C xenografts (Fig. 4C), but greater detection sensitivity of [^{18}F]-MFBG for low NET-expressing LAN1 xenografts (Fig. 4D). For SK-N-BE(2)C xenografts, the 4-hour uptake of [^{18}F]-MFBG (5.97 ± 1.86; Supplementary Table S1) is approximately 3-fold greater than the 24-hour uptake of ^{123}I-MIBG (2.10 ± 0.48; Supplementary Table S2; $P < 0.001$). For LAN1 xenografts, the 4-hour uptake of [^{18}F]-MFBG (1.72 ± 0.37; Supplementary Table S1) is also significantly greater than the 24-hour uptake of ^{123}I-MIBG (0.55 ± 0.11; Supplementary Table S2; $P < 0.001$).

Clinical imaging of neuroendocrine tumors has a long history and many comparisons between SPECT- and PET-based tracers have been performed, including ^{123}I-MIBG and ^{18}F-FDG (24), fluorodopamine (^{18}F-DA; ref. 25), and fluorodopa (^{18}F-DOPA; ref. 26). In general, ^{123}I-MIBG SPECT has been shown to be less sensitive than the PET-based radiopharmaceuticals. For example, ^{18}F-6-fluorodopamine (^{18}F-DA) has already been shown to have a higher sensitivity than ^{123}I-MIBG for the localization of metastatic pheochromocytoma (25). However, neuroendocrine tumors express different monoamine transporters (27) and the ^{18}F-labeled ligands (^{18}F-DA, ^{18}F-DOPA, [^{18}F]-MFBG, and other ^{18}F-benzylguanidine analogs) as well as ^{18}F-FDG have different patterns of tumor uptake (28). In addition, ^{18}F-DA is not an optimal imaging agent for monitoring the targeted radiotherapy of ^{131}I-MIBG because ^{18}F-DA has an accumulation pattern distinct from that of MIBG (25, 28). Detailed comparative clinical imaging studies need to be done before a conclusive statement can be made about whether an ^{18}F-labeled meta-benzylguanidine analog, such as [^{18}F]-MFBG, is a superior radiotracer for identifying NET-expressing lesions for targeted radiotherapy.

Published OnlineFirst February 26, 2014; DOI: 10.1158/1078-0432.CCR-13-1153

Although the effective radiation dose estimated for [^{18}F]-MFBG was approximately 3-fold higher than that for ^{123}I-MIBG, and approximately 4-fold lower than ^{124}I-MIBG, SPECT imaging with ^{123}I-MIBG required an approximately 4- to 5-fold higher ^{123}I-MIBG administered dose of radioactivity than that for [^{18}F]-MFBG PET imaging in our current studies. Thus, it was reasonable to project lower total radiation doses for [^{18}F]-MFBG based on translation of our mouse imaging protocol to patient imaging. For a ^{123}I-MIBG-SPECT scan, a dose of 5.2 MBq/kg body weight is recommended according to The North American Consensus Guidelines (29). Although the optimal clinical PET imaging dose of [^{18}F]-MFBG has not been determined, it is expected to be <3.7 MBq/kg. It is of note that the [^{18}F]-MFBG calculations reflect a high bladder wall deposit, which was calculated on the basis of the imaging data (whole bladder plus urine). Because [^{18}F]-MFBG is cleared faster and preferentially by the urinary system compared with ^{123}I-MIBG, its overall radiation exposure could be substantially reduced with hydration and continual or frequent emptying of the bladder. Thus, the total radiation exposure for [^{18}F]-MFBG compares favorably with that of ^{123}I-MIBG and ^{124}I-MIBG (30), especially when coupled with frequent bladder voiding.

Conclusion

Our studies show that [^{18}F]-MFBG has high specific accumulation in neuroblastoma xenografts and the magnitude of uptake reflects the expression level of NET. Although ^{123}I-MIBG has better *in vitro* uptake parameters, *in vivo* MIBG imaging is compromised by significant plasma protein binding and a comparatively slow total-body clearance. The rapid accumulation of [^{18}F]-MFBG in tumor and fast excretion from surrounding organs and the whole body allow for "early" imaging, namely, several hours following tracer administration. High-contrast images with shorter imaging acquisition times can be obtained on same day with [^{18}F]-MFBG PET, whereas ^{123}I-MIBG SPECT requires a 24-hour delay for clearance of background radioactivity. [^{18}F]-MFBG PET will facilitate imaging of children with neuroblastoma and will result in better patient compliance, due to the shorter image acquisition times.

Disclosure of Potential Conflicts of Interest

N.-K.V. Cheung has ownership interest (including patents) in Beta Glucan and 8H9. No potential conflicts of interest were disclosed by the other authors.

Authors' Contributions

Conception and design: H. Zhang, R. Huang, J.S. Lewis, R.G. Blasberg
Development of methodology: H. Zhang, R. Huang, P.B. Zanzonico, R.G. Blasberg
Acquisition of data (provided animals, acquired and managed patients, provided facilities, etc.): H. Zhang, R. Huang, N.-K.V. Cheung, P.B. Zanzonico, R.G. Blasberg
Analysis and interpretation of data (e.g., statistical analysis, biostatist \ics, computational analysis): H. Zhang, R. Huang, N.-K.V. Cheung, P.B. Zanzonico, H.T. Thaler, J.S. Lewis, R.G. Blasberg
Writing, review, and/or revision of the manuscript: H. Zhang, R. Huang, N.-K.V. Cheung, P.B. Zanzonico, H.T. Thaler, J.S. Lewis, R.G. Blasberg
Administrative, technical, or material support (i.e., reporting or organizing data, constructing databases): H. Zhang, H. Guo, J.S. Lewis
Study supervision: J.S. Lewis

Acknowledgments

The authors thank the staff of the MSKCC Small Animal Imaging Core Facility for assistance in the PET imaging, and the MSKCC Radiochemistry and Molecular Imaging Probe Core for ^{18}F production. They also thank Mr. Kuntalkumar Sevak of J.S. Lewis's lab for cell culture assistance.

Grant Support

This work was supported by NIH grant P50-CA84638 and the U.S. Department of Energy Award (DE-SC0002456, to J.S. Lewis). The MSKCC cores were supported by NIH Center grant P30-CA08748.

The costs of publication of this article were defrayed in part by the payment of page charges. This article must therefore be hereby marked *advertisement* in accordance with 18 U.S.C. Section 1734 solely to indicate this fact.

Received April 25, 2013; revised January 27, 2014; accepted February 14, 2014; published OnlineFirst February 26, 2014.

References

1. Cheung NK, Dyer MA. Neuroblastoma: developmental biology, cancer genomics and immunotherapy. Nat Rev Cancer 2013;13:397–411.
2. Kushner BH, Kramer K, Modak S, Cheung NK. Sensitivity of surveillance studies for detecting asymptomatic and unsuspected relapse of high-risk neuroblastoma. J Clin Oncol 2009;27:1041–6.
3. Goodman M, Gurney J, Smith M, Olshan A. Sympathetic nervous system tumors. Cancer Incidence and Survival among Children and Adolescents: United States SEER Program 1975–1995. Bethesda, MD: National Cancer Institute, SEER Program; 1999.
4. Brisse HJ, McCarville MB, Granata C, Krug KB, Wootton-Gorges SL, Kanegawa K, et al. Guidelines for imaging and staging of neuroblastic tumors: consensus report from the International Neuroblastoma Risk Group Project. Radiology 2011;261:243–57.
5. Taggart DR, Han MM, Quach A, Groshen S, Ye W, Villablanca JG, et al., Comparison of iodine-123 metaiodobenzylguanidine (MIBG) scan and [^{18}F]fluorodeoxyglucose positron emission tomography to evaluate response after iodine-131 MIBG therapy for relapsed neuroblastoma. J Clin Oncol 2009;27:5343–9.
6. Pacholczyk T, Blakely RD, Amara SG. Expression cloning of a cocaine- and antidepressant-sensitive human noradrenaline transporter. Nature 1991;350:350–4.
7. Vaidyanathan G. Meta-iodobenzylguanidine and analogues: chemistry and biology. Q J Nucl Med Mol Imaging 2008;52:351–68.
8. Grunwald F, Ezziddin S. ^{131}I-metaiodobenzylguanidine therapy of neuroblastoma and other neuroendocrine tumors. Semi Nucl Med 2010;40:153–63.
9. Rufini V, Shulkin B. The evolution in the use of MIBG in more than 25 years of experimental and clinical applications. Q J Nucl Med Mol Imaging 2008;52:341–50.
10. Monclair T, Brodeur GM, Ambros PF, Brisse HJ, Cecchetto G, Holmes K, et al. The International Neuroblastoma Risk Group (INRG) staging system: an INRG Task Force report. J Clin Oncol 2009;27:298–303.
11. Dessner DA, DiPietro MA, Shulkin BL. MIBG detection of hepatic neuroblastoma: correlation with CT, US and surgical findings. Pediatr Radiol 1993;23:276–80.
12. Pfluger T, Schmied C, Porn U, Leinsinger G, Vollmar C, Dresel S, et al. Integrated imaging using MRI and ^{123}I metaiodobenzylguanidine scintigraphy to improve sensitivity and specificity in the diagnosis of pediatric neuroblastoma. AJR Am J Roentgenol 2003;181:1115–24.
13. Melzer HI, Coppenrath E, Schmid I, Albert MH, von Schweinitz D, Tudball C, et al. ^{123}I-MIBG scintigraphy/SPECT versus ^{18}F-FDG PET in

Published OnlineFirst February 26, 2014; DOI: 10.1158/1078-0432.CCR-13-1153

paediatric neuroblastoma. Eur J Nucl Med Mol Imaging 2011;38: 1648–58.
14. Tai YC, Ruangma A, Rowland D, Siegel S, Newport DF, Chow PL, et al. Performance evaluation of the microPET focus: a third-generation microPET scanner dedicated to animal imaging. J Nucl Med 2005;46: 455–63.
15. Cohn SL, Pearson AD, London WB, Monclair T, Ambros PF, Brodeur GM, et al. The International Neuroblastoma Risk Group (INRG) classification system: an INRG Task Force report. J Clin Oncol 2009;27: 289–97.
16. Sisson JC, Yanik GA. Theranostics: evolution of the radiopharmaceutical meta-iodobenzylguanidine in endocrine tumors. Semi Nucl Med 2012;42:171–84.
17. Matthay KK, George RE, Yu AL. Promising therapeutic targets in neuroblastoma. Clin Cancer Res 2012;18:2740–53.
18. Jacobson AF, Deng H, Lombard J, Lessig HJ. Black RR, ^{123}I-metaiodobenzylguanidine scintigraphy for the detection of neuroblastoma and pheochromocytoma: results of a meta-analysis. J Clin Endocrinol Metab 2010;95:2596–606.
19. Messina JA, Cheng SC, Franc BL, Charron M, Shulkin B, To B, et al. Evaluation of semi-quantitative scoring system for metaiodobenzylguanidine (mIBG) scans in patients with relapsed neuroblastoma. Pediatr Blood Cancer 2006;47:865–74.
20. Vaidyanathan G, Affleck DJ, Zalutsky MR. (4-[^{18}F]fluoro-3-iodobenzyl) guanidine, a potential MIBG analogue for positron emission tomography. J Med Chem 1994;37:3655–62.
21. Lee BC, Paik JY, Chi DY, Lee KH, Choe YS, Potential and practical adrenomedullary PET radiopharmaceuticals as an alternative to m-iodobenzylguanidine: m-(omega-[^{18}F]fluoroalkyl)benzylguanidines. Bioconjug Chem 2004;15:104–11.
22. Yu M, Bozek J, Lamoy M, Guaraldi M, Silva P, Kagan M, et al. Evaluation of LMI1195, a novel ^{18}F-labeled cardiac neuronal PET imaging agent, in cells and animal models. Circ Cardiovasc Imaging 2011;4:435–43.
23. Zhang H, Huang R, Pillarsetty N, Thorek DL, Vaidyanathan G, Serganova I, et al. Synthesis and evaluation of (18)F-labeled benzylguanidine analogs for targeting the human norepinephrine transporter. Eur J Nucl Med Mol Imaging 2014;41:322–32.
24. Sharp SE, Shulkin BL, Gelfand MJ, Salisbury S, Furman WL. ^{123}I-MIBG scintigraphy and ^{18}F-FDG PET in neuroblastoma. J Nucl Med 2009;50:1237–43.
25. Ilias I, Chen CC, Carrasquillo JA, Whatley M, Ling A, Lazurova I, et al. Comparison of 6–^{18}F-fluorodopamine PET with ^{123}I-metaiodobenzylguanidine and ^{111}in-pentetreotide scintigraphy in localization of nonmetastatic and metastatic pheochromocytoma. J Nucl Med 2008;49: 1613–9.
26. Kauhanen S, Seppanen M, Ovaska J, Minn H, Bergman J, Korsoff P, et al. The clinical value of [^{18}F]fluoro-dihydroxyphenylalanine positron emission tomography in primary diagnosis, staging, and restaging of neuroendocrine tumors. Endoc Relat Cancer 2009;16: 255–65.
27. Anlauf M, Eissele R, Schafer MK, Eiden LE, Arnold R, Pauser U, et al. Expression of the two isoforms of the vesicular monoamine transporter (VMAT1 and VMAT2) in the endocrine pancreas and pancreatic endocrine tumors. J Histochem Cytochem 2003;51:1027–40.
28. Timmers HJ, Chen CC, Carrasquillo JA, Whatley M, Ling A, Havekes B, et al. Comparison of ^{18}F-fluoro-L-DOPA, ^{18}F-fluoro-deoxyglucose, and ^{18}F-fluorodopamine PET and ^{123}I-MIBG scintigraphy in the localization of pheochromocytoma and paraganglioma. J Clin Endocrinol Metab 2009;94:4757–67.
29. Gelfand MJ, Parisi MT, Treves ST. Pediatric nuclear medicine dose reduction W, pediatric radiopharmaceutical administered doses: 2010 North American consensus guidelines. J Nucl Med 2011;52: 318–22.
30. Lee CL, Wahnishe H, Sayre GA, Cho HM, Kim HJ, Hernandez-Pampaloni M, et al. Radiation dose estimation using preclinical imaging with ^{124}I-metaiodobenzylguanidine (MIBG) PET. Med Phys 2010;37: 4861–7.

Published OnlineFirst February 26, 2014; DOI: 10.1158/1078-0432.CCR-13-1153

Clinical Cancer Research

Imaging the Norepinephrine Transporter in Neuroblastoma: A Comparison of [^{18}F]-MFBG and ^{123}I-MIBG

Hanwen Zhang, Ruimin Huang, Nai-Kong V. Cheung, et al.

Clin Cancer Res 2014;20:2182-2191. Published OnlineFirst February 26, 2014.